# Optimal MISO UWB Pre-Equalizer Design with Spectral Mask Constraints

Amir-Hamed Mohsenian-Rad, Jan Mietzner, Robert Schober, and Vincent W.S. Wong
Department of Electrical and Computer Engineering, University of British Columbia, Vancouver, Canada
E-mail: {hamed, rschober, vincentw}@ece.ubc.ca, jan.mietzner@ieee.org

***Abstract*— In this paper, we propose a novel optimization-based pre-equalization filter (PEF) design for multiple-input single-output (MISO) direct-sequence ultra-wideband (DS-UWB) systems with pre-Rake combining. The key feature in our design is that we explicitly take into account *spectral mask* constraints which are usually imposed by telecommunications regulation and standardization bodies. This avoids the need for an inefficient *power back-off*, which is necessary for existing pre-equalizer and pre-Rake designs that are designed solely based on average transmit power constraints. Simulation results confirm that the proposed PEF design leads to significant performance gains over UWB PEF structures without any explicit spectral mask considerations. Furthermore, the use of multiple transmit antennas is shown to provide substantial combining gains compared to single-antenna transmitter structures. We also investigate the impact of certain system and optimization parameters on the performance of the proposed PEF design.**

***Index Terms*— Multiple antennas, ultra-wideband communication, pre-equalization, pre-Rake combining, spectral mask constraints, semi-definite programming.**

## I. Introduction

Ultra-wideband (UWB) is an emerging spectral underlay technology for high-rate short-range transmission, e.g., for wireless personal area networks (WPANs). Due to their extremely large bandwidth, UWB systems can resolve even dense multipath components such that Rake combining can be used at the receiver to significantly reduce the negative impacts of fading in the received signal [1]. However, for many UWB applications, the receiver is a portable device with limited signal processing capabilities, making the implementation of Rake combiners with a sufficiently large number of fingers challenging in practice.

To overcome this problem, a promising approach is to move computational complexity from the receiver to the more powerful transmitter (e.g., an access point). In this regard, *pre-Rake combining* can be used [2]–[4]. Pre-Rake combining exploits the reciprocity of the UWB radio channel, which has recently been confirmed experimentally in [5]. Ideally, with pre-Rake combining at the transmitter, channel estimation, diversity combining, and equalization are avoided at the receiver, and a simple symbol-by-symbol detector can be used [3], [6].

However, pre-Rake combining has some serious drawbacks. In particular, for the *long* channel impulse responses (CIRs), which are typical for UWB applications, it may entail a relatively high error floor if simple symbol-by-symbol detection is applied at the receiver [2]. To remedy this problem, while still keeping the receiver simple, *pre-equalization* can be used at the transmitter to effectively decrease the residual intersymbol interference (ISI) at the receiver [7], [8].

Most of the previous works on pre-Rake and pre-equalizer design for UWB systems (e.g. in [2]–[9]) include side constraints to limit the overall (average) transmit power. However, prior studies do not include constraints to limit the *power spectral density* (PSD) of the transmitted UWB signals. This can severely affect the overall system performance, as most of the telecommunication regulation bodies, e.g., the US Federal Communications Commission (FCC), impose restricted *spectral masks* to limit UWB interference on incumbent legacy narrowband receivers. In such a setting, the existing UWB pre-filtering techniques can be far from optimal in practice, as they require an appropriate *power back-off* so that the spectral masks are not violated.

In this paper, we propose a novel *pre-equalization filter* (PEF) design for direct-sequence (DS) UWB systems [10], which explicitly takes into account spectral mask constraints.[1] In particular, we consider the multiple-input single-output (MISO) case and show that multiple transmit antennas can be used efficiently to provide substantial combining gains at the receiver. This is a very appealing feature, given that spectral mask regulations are usually very tight, i.e., the received signal power should be maximized by all means.[2] We first formulate an elaborate *non-convex* optimization problem with the PEF coefficients being the optimization variables. We then employ a *semi-definite relaxation* technique, which allows us to find a close-to-optimal PEF design. Our simulation results confirm that our proposed PEF scheme leads to significant performance gains over competing schemes without spectral mask considerations. To the best of our knowledge, this work is the first to explicitly consider spectral mask constraints for pre-filter design in DS-UWB systems.[3] We note that the PEF designs in this paper are significantly different from previous work in the literature on UWB *pulse-shaping* with spectral mask considerations, e.g. in [13], which does not address pre-equalization or residual ISI limitation.

*Paper Organization*: The remainder of this paper is organized as follows. The system model under consideration is presented in Section II. We then formulate the PEF optimization problem in Section III. An efficient algorithm to solve this optimization problem is provided in Section IV. Simulation results are given in Section V and, finally, the paper is concluded in Section VI.

*Notation*: $\mathcal{E}\{\cdot\}$, $[\cdot]^T$, $(\cdot)^*$, $[\cdot]^H$, $\Re\{\cdot\}$, $\lceil\cdot\rceil$, $\delta(\cdot)$, and $*$ denote statistical expectation, transposition, complex conjugation, Hermitian transposition, the real part of a complex number, the ceiling function, the Dirac delta function, and linear convolution, respectively. Also $X(e^{j\omega}) \triangleq \mathcal{F}\{x[k]\} = \sum_{k=-\infty}^{\infty} x[k]e^{-j\omega k}$, $X(j\Omega) \triangleq \mathcal{F}\{x(t)\} = \int_{-\infty}^{+\infty} x(t)e^{-j\Omega t}dt$, $\Phi_{xx}(e^{j\omega}) \triangleq \mathcal{F}\{\phi_{xx}[\tau]\} = \sum_{\tau=-\infty}^{\infty} \phi_{xx}[\tau]e^{-j\omega\tau}$, and $\phi_{xx}[\tau] \triangleq \mathcal{E}\{x[k]x^*[k-\tau]\}$ denote the *discrete–time* Fourier transform, the *continuous–time* Fourier transform, the PSD, and the au-

[1] The PEF design techniques proposed in this paper could be easily extended to impulse-radio-based UWB (IR-UWB) systems [11] as well.

[2] For example, the FCC spectral mask for outdoor UWB transmissions in the 3.1-10.6 GHz band is as low as $-41$ dBm/MHz, corresponding to an overall transmission power of just $73.3\,\mu$W given a system bandwidth of 1 GHz. Because of these limitations, it is indispensable to capture as much signal energy at the receiver as possible.

[3] The current paper constitutes an extension of our earlier work [12], which focused on the single transmit-antenna case.

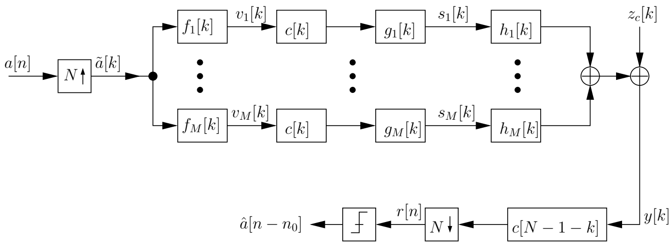


Fig. 1. Block diagram of a MISO DS-UWB system with pre-equalization and pre-Rake combining ($M$ transmit antennas and one receive antenna).

tocorrelation function, respectively. Depending on the context, $x[k]$ represents either a sequence or the $k$th element of a sequence. Finally, $\mathrm{diag}(\cdot)$ denotes a block-diagonal matrix.

## II. System Model

Consider the discrete-time complex baseband model of a (single-user) MISO DS-UWB system [10] with $M$ transmit antennas and a single receive antenna, as depicted in Fig 1. Throughout this paper, we denote the symbol duration by $T_s$ and the chip duration by $T_c = T_s/N$, where $N$ is the *spreading factor*.

*Transmitter Structure*: At the transmitter, a train of independent and identically distributed (i.i.d.) data symbols $a[n] \in \{\pm 1\}$ is first up-sampled by the spreading factor $N$ to yield

$$\tilde{a}[k] = \begin{cases} a[n], & \text{if } k = N\,n, \\ 0, & \text{if } k \neq N\,n. \end{cases} \quad (1)$$

At transmit antenna $m$ $(1 \leq m \leq M)$, the up-sampled data sequence $\tilde{a}[k]$ is then filtered with a PEF $f_m[k]$ of length $L_f$. We will optimize the PEFs $f_1[k], ..., f_M[k]$ for minimization of the amount of residual ISI at the receiver in Sections III and IV. The filter output signal at transmit antenna $m$ is obtained as

$$v_m[k] \triangleq f_m[k] * \tilde{a}[k] = \sum_{l=0}^{L_f-1} f_m[l]\tilde{a}[k-l]. \quad (2)$$

The resulting sequence $v_m[k]$ is filtered once more by a (real-valued) spreading sequence $c[k]$, which is normalized such that $\sum_{k=0}^{N-1} |c[k]|^2 = 1$, and a pre-Rake filter $g_m[k]$ of length $L_g$. The resulting transmitted sequence $s_m[k]$ is given by

$$s_m[k] = v_m[k] * \tilde{g}_m[k] = \sum_{i=-\infty}^{\infty} v_m[i]\tilde{g}_m[k-i], \quad (3)$$

where

$$\tilde{g}_m[k] \triangleq c[k] * g_m[k] = \sum_{i=0}^{N-1} c[i] g_m[k-i] \quad (4)$$

includes the combined effects of the pre-Rake filter $g_m[k]$ and the spreading sequence $c[k]$. Here, we do not impose any restrictions on $c[k]$ or $g_m[k]$. If a spreading sequence is not applied, e.g. as in [2], [3], [5], we simply have $c[0] = 1$ and $c[k] = 0$, $1 \leq k < N$. In general, $g_m[k]$ depends on the corresponding UWB CIR $h_m[k]$ (associated with the $m$th transmit antenna), which has length $L_h$.[4] In this paper, we assume that an *all-pre-Rake* (also called *time-reversal*) filter is employed at each transmit antenna $m$, i.e.,

$$g_m[k] \triangleq h_m^*[L_h - k - 1] \qquad (0 \leq k < L_g,\ L_g = L_h). \quad (5)$$

*Channel Model*: The equivalent baseband discrete-time CIR

$$h_m[k] \triangleq g_T(t) * h_m(t) * g_R(t)|_{kT_c} \quad (6)$$

associated with the $m$th transmit antenna contains the combined effects of a square-root Nyquist transmit filter $g_T(t)$ [10], the continuous-time CIR $h_m(t)$, and the receive filter $g_R(t)$, sampled at chip interval $T_c$. For the wireless channel, we adopt the proposed extension of the IEEE 802.15.3a channel model [14], [15] to multiple antennas [16]. Consequently, the passband version $h'_m(t)$ of the baseband CIR $h_m(t)$ consists of $L_{c,m}$ clusters of $L_{r,m}$ rays and is modeled as

$$h'_m(t) = \vartheta_m \sum_{l=1}^{L_{c,m}} \sum_{k=1}^{L_{r,m}} \xi_{k,l,m} \delta(t - T_{l,m} - \tau_{k,l,m}), \quad (7)$$

where $T_{l,m}$ is the delay of the $l$th cluster, $\tau_{k,l,m}$ is the delay of the $k$th ray of the $l$th cluster, $\xi_{k,l,m}$ is the random multipath gain coefficient, and $\vartheta_m$ models the lognormal shadowing. In [14], [15], four parameter sets for the various channel model (CM) parameters in (7) are specified. The resulting channel models are known as CM1, CM2, CM3, and CM4. They represent different usage scenarios and entail different amounts of ISI. Measurements reported in [16] have confirmed that while $T_{l,m}$, $\tau_{k,l,m}$, and $\rho_{k,l,m}$ are independent across antennas, the lognormal terms $\vartheta_m$ are mutually correlated. Hence, we employ a Kronecker correlation model for the UWB CIRs associated with different transmit antennas, as suggested in [16].

*Receiver Structure*: The received sum signal

$$y[k] = \sum_{m=1}^{M} \sum_{l=0}^{L_h-1} h_m[l] s_m[k-l] + w_c[k], \quad (8)$$

including chip-level additive white Gaussian noise (AWGN) samples $w_c[k]$ with variance $\sigma_c^2 = \mathcal{E}\{|w_c[k]|^2\}$, is filtered using the time-reversed spreading sequence $c[N-1-k]$. Then, down-sampling at times $k = Nn + k_0$ is performed, where $k_0$ denotes the sampling phase. The resulting receiver output signal $r[n]$ can be expressed as

$$r[n] = \sum_{m=1}^{M} \sum_{l=-\infty}^{\infty} b_m[Nl + k_0] a[n-l] + w_s[n], \quad (9)$$

where

$$b_m[k] \triangleq f_m[k] * q_m[k] = \sum_{i=0}^{L_f-1} f_m[i]\, q_m[k-i] \quad (10)$$

with overall CIR

$$q_m[k] = \tilde{g}_m[k] * \tilde{h}_m[k] = \sum_{i=0}^{L_g+N-2} \tilde{g}_m[i]\tilde{h}_m[k-i], \quad (11)$$

and

$$w_s[n] = \sum_{i=0}^{N-1} c[i] w_c[N(n-1) + k_0 + i + 1] \quad (12)$$

[4]For simplicity, we assume that the UWB CIRs $h_m[k]$, $1 \leq m \leq M$, all have the same length $L_h$. In the case of unequal CIR lengths, $L_h$ represents the maximum length, and shorter CIRs are padded with zeros.

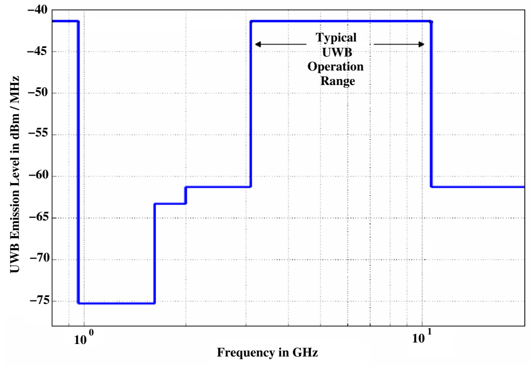


Fig. 2. FCC spectral mask for UWB transmissions in outdoor environments. A typical operational range for UWB systems is the 3.1-10.6 GHz band.

denotes the symbol-level noise. Here, $\tilde{h}_m[k]$ includes the combined effects of the channel filter $h_m[k]$ and the time-reversed spreading sequence $c[N-1-k]$:

$$\tilde{h}_m[k] \triangleq h_m[k] * c[N-1-k] = \sum_{i=0}^{N-1} c[i] h_m[k+i-(N-1)]. \tag{13}$$

Note that $w_s[n]$ is also AWGN noise with variance

$$\sigma_s^2 \triangleq \mathcal{E}\{|w_s[n]|^2\} = \sigma_c^2 \sum_{i=0}^{N-1} |c[i]|^2 = \sigma_c^2. \tag{14}$$

Since our goal is to design a UWB system with *minimal receiver complexity*, no additional filtering is applied at the receiver, and symbol decisions are made according to

$$\hat{a}[n-n_0] = \mathrm{sign}\{\Re\{r[n]\}\}, \tag{15}$$

where $\hat{a}[n-n_0]$ is the estimate for $a[n-n_0]$, $n_0$ denotes the decision delay, and $\mathrm{sign}\{x\} = 1$ if $x \geq 0$ and $\mathrm{sign}\{x\} = -1$ otherwise. Note that *no* equalizer is used at the receiver.

Next, we will optimize the PEFs $f_m[k]$ ($m=1, ..., M$) with respect to the following design goals:

- *Obeying spectral mask limitations:* Throughout the entire operational bandwidth $B_s$, the transmitted (sum) PSD must obey spectral mask limitations that are imposed by telecommunications regulation bodies in order to prevent interference to incumbent legacy narrowband receivers. As an example, the FCC spectral mask for outdoor communications is shown in Fig. 2 [17].
- *Focusing of channel energy:* Since we assume that *no* equalizer is used at the receiver, most of the energy of the overall CIRs $q_m[k]$ must be concentrated in a *single* channel tap. The amount of residual ISI must be strictly limited, in order to avoid error floors.
- *Limiting average transmit power:* The overall average transmission power of the MISO DS-UWB system must be smaller than or equal to some upper limit $P^{\max}$ (e.g. due to hardware limitations).

In the next section, we propose an elaborate optimization framework for the design of efficient PEFs subject to the above constraints. We will provide an algorithm to solve the resulting optimization problem in Section IV.

## III. Problem Formulation

It is convenient to first rewrite (9) in vector form as

$$r[n] = \sum_{m=1}^{M} (\mathbf{B}_m \, \mathbf{f}_m)^H \mathbf{a}[n] + w_s[n], \tag{16}$$

where

$$\mathbf{a}[n] \triangleq [a[n] \, \ldots \, a[n-L_t+1]]^T \tag{17}$$

with

$$L_t \triangleq L_q + L_f - 1 \tag{18}$$

and

$$L_q \triangleq \lceil (L_g + L_h + 2N - 3)/N \rceil \tag{19}$$

being the lengths of the impulse response of the overall system (including PEF $f_m[k]$) and of the sampled overall CIR $q_m[Nn+k_0]$, respectively. Moreover, we have introduced the definition

$$\mathbf{f}_m \triangleq [f_m[0] \, \ldots \, f_m[L_f-1]]^H. \tag{20}$$

Finally, $\mathbf{B}_m$ is an $L_t \times L_f$ matrix, the $i$th row of which is equal to the $(N(i-1)+1)$th row of an $L_b \times L_f$ *column-circulant* matrix $\tilde{\mathbf{B}}_m$ with vector

$$[b_m[k_0] \; b_m[1+k_0] \, \ldots \, b_m[L_g+L_h-1+k_0] \; \mathbf{0}_{L_f-1}^T]^H$$

as its first column, where

$$L_b \triangleq L_g + L_h + L_f + 2N - 4 \tag{21}$$

and $\mathbf{0}_{L_f-1}$ denotes an $(L_f-1) \times 1$ vector with all entries equal to zero. We can rewrite (16) in a more compact form according to

$$r[n] = (\mathbf{B}\,\mathbf{f})^H \mathbf{a}[n] + w_s[n], \tag{22}$$

where

$$\mathbf{B} \triangleq [\mathbf{B}_1, \mathbf{B}_2, \cdots, \mathbf{B}_M] \tag{23}$$

is of size $L_t \times ML_f$ and

$$\mathbf{f} \triangleq \left[\mathbf{f}_1^T, \mathbf{f}_2^T, \cdots, \mathbf{f}_M^T\right]^T. \tag{24}$$

Next, we study PEF design aspects.

*Spectral Mask Constraints:* We first note that our system model is in *discrete–time*, while the spectral mask is usually defined in *continuous–time*. Let $\Omega$ and $\omega$ denote the angular frequency associated with the continuous–time and discrete–time Fourier transform, respectively. We define $\Omega_{\min}$ and $\Omega_{\max}$ as the minimum and maximum frequencies used by the UWB system (e.g., $\Omega_{\min} = 2\pi \times 3.5$ GHz and $\Omega_{\max} = 2\pi \times 4.5$ GHz [10]). Thus $B_s = \Omega_{\max} - \Omega_{\min}$ denotes the total bandwidth used by the designed UWB system. Also let $m(\Omega)$ denote the imposed spectral mask. For example, in the case of the FCC spectral mask we have $m(\Omega) = -41.3$ dBm/MHz for any $\Omega_{\min} \leq \Omega \leq \Omega_{\max}$, cf. Fig. 2, where the radiated emissions are measured using a resolution bandwidth of 1 MHz [17]. Therefore, we need to ensure that we obey the spectral mask within every 1 MHz of occupied bandwidth. Let $\Omega_1, \ldots, \Omega_K$ denote $K \triangleq \frac{B_s}{1\text{MHz}} + 1$ discrete frequency levels which uniformly spread out over the bandwidth $B_s$. Clearly, we have $\Delta\,\Omega = \Omega_2 - \Omega_1 = \ldots = \Omega_K - \Omega_{K-1} = 2\pi \times 1$ MHz. For each $\mu = 1, \ldots, K$ it is required that the transmitted sum power spectra obeys the spectral mask, i.e.,

$$\sum_{m=1}^{M} \int_{\omega_\mu - \frac{\Delta\omega}{2}}^{\omega_\mu + \frac{\Delta\omega}{2}} \left| G_T\left(j\frac{\omega}{T_c}\right)\right|^2 \Phi_{s_m s_m}(e^{j\omega}) \, d\,\omega \tag{25}$$

$$\stackrel{!}{\leq} \int_{\Omega_\mu - \frac{\Delta\Omega}{2}}^{\Omega_\mu + \frac{\Delta\Omega}{2}} m(\Omega) \, d\,\Omega,$$

where $\omega_\mu \triangleq T_c\,\Omega_\mu$ [18, Ch. 1.7], $\Delta\omega \triangleq T_c\,\Delta\Omega$, $G_T(j\,\frac{\omega}{T_c}) = \mathcal{F}\{g_T(t)\}$, and $\Phi_{s_m s_m}(e^{j\omega})$ denotes the PSD for transmitted signal $s_m[k]$. Recall that $g_T(t)$ is the transmit filter. We can show that

$$\Phi_{s_m s_m}(e^{j\omega}) = \left|\tilde{G}_m(e^{j\omega})\right|^2 \; \Phi_{\tilde{v}_m \tilde{v}_m}(e^{j\omega}), \tag{26}$$

where $\tilde{G}_m(e^{j\omega}) = \mathcal{F}\{\tilde{g}_m[k]\}$. We also have

$$\Phi_{\tilde{v}_m \tilde{v}_m}(e^{j\omega}) = \left|F_m(e^{j\omega})\right|^2 \; \Phi_{\tilde{a}\tilde{a}}(e^{j\omega}) = \left|F_m(e^{j\omega})\right|^2, \tag{27}$$

where $F_m(e^{j\omega}) = \mathcal{F}\{f_m[k]\}$ and $\Phi_{\tilde{a}\tilde{a}}(e^{j\omega}) \equiv 1$ due to the i.i.d. assumption for the data symbols $a[n]$. From (26) and (27), and assuming that the spectral mask $m(\Omega)$ and PSD $|G_T(j\frac{\omega}{T_c})|^2 \;\; \Phi_{s_m s_m}(e^{j\omega})$ are practically constant over $\Omega_\mu - \frac{\Delta\Omega}{2} \leq \Omega \leq \Omega_\mu + \frac{\Delta\Omega}{2}$ and $\omega_\mu - \frac{\Delta\omega}{2} \leq \omega \leq \omega_\mu + \frac{\Delta\omega}{2}$, respectively, for each $\mu = 1,\ldots,K$ inequality (25) becomes

$$\sum_{m=1}^{M} \lambda_m(\omega_\mu) \left|F_m(e^{j\omega_\mu})\right|^2 \;\leq\; m(\Omega_\mu), \tag{28}$$

where

$$\lambda_m(\omega_\mu) \triangleq T_c \; \left|\tilde{G}_m(e^{j\omega_\mu})\right|^2 \; \left|G_T\left(j\,\frac{\omega_\mu}{T_c}\right)\right|^2. \tag{29}$$

Clearly, we can ensure (28) by tuning the coefficients in the PEFs $\mathbf{f}_1,\ldots,\mathbf{f}_M$. The spectral mask constraints in (28) can be written in vector form, using

$$\left|F_m(e^{j\omega})\right|^2 = \mathbf{f}_m^H \,\mathbf{d}(\omega)\,\mathbf{d}^H(\omega)\,\mathbf{f}_m, \tag{30}$$

where $\mathbf{d}(\omega) \triangleq [1 \;\, e^{j\omega} \;\, e^{j\omega\cdot 2} \;\, \ldots \;\, e^{j\omega\cdot(L_f-1)}]^T$. Therefore, the spectral mask in (28) imposes $K$ inequality constraints on the PEFs $\mathbf{f}_1,\ldots,\mathbf{f}_M$ as

$$\sum_{m=1}^{M} \lambda_m(\omega_\mu)\,\mathbf{f}_m^H\,\mathbf{d}(\omega_\mu)\,\mathbf{d}^H(\omega_\mu)\,\mathbf{f}_m \leq m(\Omega_\mu) \tag{31}$$

($\mu = 1,\ldots,K$). Note that the terms $\lambda_m(\omega_\mu)$, $m = 1,\ldots,M$, are *fixed* for each $\mu = 1,\ldots,K$ as far as the design of the PEFs is concerned. We can rewrite (31) in a more compact form according to

$$\mathbf{f}^H\,\mathbf{D}(\omega_\mu)\,\mathbf{f} \leq m(\Omega_\mu), \tag{32}$$

where

$$\mathbf{D}(\omega) \triangleq \mathrm{diag}\left(\lambda_1(\omega)\,\mathbf{d}(\omega)\,\mathbf{d}^H(\omega), \cdots, \lambda_M(\omega)\,\mathbf{d}(\omega)\,\mathbf{d}^H(\omega)\right). \tag{33}$$

*Energy Concentration:* Since we assume that *no* equalizer is used at the receiver, it is required that for each received symbol, most of the channel energy is concentrated in a *single* channel tap. Considering (16), let $\mathbf{B}_{m,pre}$ denote the submatrix of $\mathbf{B}_m$ consisting of the first $\eta_{pre}$ rows. Also let $\mathbf{B}_{m,post}$ denote the submatrix of $\mathbf{B}_m$ consisting of the last $\eta_{post}$ rows. Here, $\eta_{pre}$ and $\eta_{post}$ are selected such that $\eta_{pre} + \eta_{post} + 1 = L_t$, where $L_t$ is as in (18). We can rewrite $\mathbf{B}_m$ as

$$\mathbf{B}_m = \begin{bmatrix} \mathbf{B}_{m,pre} \\ \mathbf{B}_{m,0} \\ \mathbf{B}_{m,post} \end{bmatrix}. \tag{34}$$

Here, $\mathbf{B}_{m,0}$ denotes the $(\eta_{pre}+1)^{\text{th}}$ row of matrix $\mathbf{B}_m$. We can thus rewrite (16) as

$$r[n] \;=\; \sum_{m=1}^{M}\Big[(\mathbf{B}_{m,0}\,\mathbf{f}_m)^*\,a_0[n] + (\mathbf{B}_{m,pre}\,\mathbf{f}_m)^H\,\mathbf{a}_{pre}[n] + (\mathbf{B}_{m,post}\,\mathbf{f}_m)^H\,\mathbf{a}_{post}[n]\Big] + w_s[n], \tag{35}$$

where $a_0[n] \triangleq a[n-n_0] = a[n-\eta_{pre}]$, $\mathbf{a}_{pre}[n] \triangleq [a[n] \; \ldots \; a[n-\eta_{pre}-1]]^T$, and $\mathbf{a}_{post}[n] \triangleq [a[n-\eta_{pre}+1] \; \ldots \; a[n-L_t+1]]^T$. We can rewrite (35) in a more compact form according to

$$\begin{aligned} r[n] \;&=\; (\mathbf{B}_0\,\mathbf{f})^*\,a_0[n] + (\mathbf{B}_{pre}\,\mathbf{f})^H\,\mathbf{a}_{pre}[n] \\ &\quad + (\mathbf{B}_{post}\,\mathbf{f})^H\,\mathbf{a}_{post}[n] + w_s[n], \end{aligned} \tag{36}$$

where

$$\mathbf{B}_0 \triangleq [\mathbf{B}_{1,0}, \cdots, \mathbf{B}_{M,0}], \tag{37}$$

$$\mathbf{B}_{pre} \triangleq [\mathbf{B}_{1,pre}, \cdots, \mathbf{B}_{M,pre}], \tag{38}$$

$$\mathbf{B}_{post} \triangleq [\mathbf{B}_{1,post}, \cdots, \mathbf{B}_{M,post}]. \tag{39}$$

In order to achieve a low bit error rate (BER), we have to concentrate most of the energy of the overall CIR $\mathbf{B}\,\mathbf{f}$ in a *single* high energy tap $\mathbf{B}_0\,\mathbf{f}$, while keeping the residual ISI caused by the terms $(\mathbf{B}_{pre}\mathbf{f})^H\,\mathbf{a}_{pre}[n]$ and $(\mathbf{B}_{post}\mathbf{f})^H\,\mathbf{a}_{post}[n]$ in (36) as small as possible. This introduces the following constraint on the PEF coefficients:

$$\mathbf{f}^H\mathbf{B}_{pre}^H\mathbf{B}_{pre}\mathbf{f} + \mathbf{f}^H\mathbf{B}_{post}^H\mathbf{B}_{post}\mathbf{f} \leq \alpha, \tag{40}$$

where $\alpha$ is a design parameter which imposes an upper bound for the amount of residual ISI at the receiver. One possible choice that leads to a desirable system performance (as shown in Section V) is to set $\alpha = \sigma_s^2$ in order to limit the residual ISI to be less than or equal to the noise variance. We notice that our design goal regarding the energy concentration in a single tap can also be interpreted in terms of the *signal-to-interference-plus-noise-ratio* (SINR) for each symbol:

$$\text{SINR} \triangleq \frac{\mathbf{f}^H\mathbf{B}_0^H\mathbf{B}_0\mathbf{f}}{\mathbf{f}^H\mathbf{B}_{pre}^H\mathbf{B}_{pre}\mathbf{f} + \mathbf{f}^H\mathbf{B}_{post}^H\mathbf{B}_{post}\mathbf{f} + \sigma_s^2}. \tag{41}$$

Clearly, by maximizing the term $\mathbf{f}^H\mathbf{B}_0^H\mathbf{B}_0\mathbf{f}$, while limiting $\mathbf{f}^H\mathbf{B}_{pre}^H\mathbf{B}_{pre}\mathbf{f} + \mathbf{f}^H\mathbf{B}_{post}^H\mathbf{B}_{post}\mathbf{f}$, we can increase the SINR and thus obtain a better (i.e., lower) BER.

*Power Constraint:* Further to the PSD constraints, we can also limit the overall *average* transmission power. By taking similar steps as in [8, Appendix A], we can show that the power constraint can be formulated as

$$\sum_{m=1}^{M} \mathcal{E}\{|s_m[k]|^2\} = \mathbf{f}^H\,\boldsymbol{\Upsilon}\,\mathbf{f} \leq P^{\max}, \tag{42}$$

where constant $P^{\max} > 0$ represents the maximum transmission power. Moreover,

$$\boldsymbol{\Upsilon} \triangleq \mathrm{diag}\left(\boldsymbol{\Upsilon}_1, \cdots, \boldsymbol{\Upsilon}_M\right), \tag{43}$$

where $\boldsymbol{\Upsilon}_m$, $1 \leq m \leq M$, is a Hermitian Toeplitz matrix with vector

$$[\varphi_m[0], \varphi_m[1], \ldots, \varphi_m[(L_f-1)]] \tag{44}$$

in its first row, where $\varphi_m[k] \triangleq \tilde{g}_m[k] * \tilde{g}_m[-k]$.

*Optimization Problem:* Combining our considerations regarding spectral mask, energy concentration, and average transmit power, the proposed PEF design is obtained as the optimal solution of the following optimization problem over *complex-valued* vector variable $\mathbf{f}$:

$$\begin{aligned} \max_{\mathbf{f}} \quad & \mathbf{f}^H\mathbf{B}_0^H\mathbf{B}_0\mathbf{f} \\ \text{s.t.} \quad & \mathbf{f}^H\left(\mathbf{B}_{pre}^H\mathbf{B}_{pre} + \mathbf{B}_{post}^H\mathbf{B}_{post}\right)\mathbf{f} \leq \alpha \\ & \mathbf{f}^H\mathbf{D}(\omega_1)\mathbf{f} \leq m(\Omega_1) \\ & \vdots \\ & \mathbf{f}^H\mathbf{D}(\omega_K)\mathbf{f} \leq m(\Omega_K) \\ & \mathbf{f}^H\,\boldsymbol{\Upsilon}\,\mathbf{f} \leq P^{\max}. \end{aligned} \tag{45}$$

Problem (45) is a *non-concave* quadratic maximization problem as the objective function $\mathbf{f}^H \mathbf{B}_0^H \mathbf{B}_0 \mathbf{f}$ is *not* concave in $\mathbf{f}$. Thus, the standard gradient-based methods (cf. [19]) cannot be used for solving it. Moreover, problem (45) has many nonlinear constraints and is thus difficult to solve in closed-form. Nevertheless, we can find a *close-to-optimal* solution for optimization problem (45) using a semi-definite relaxation technique, as we will explain in Section IV. In particular, we arrive at a *semi-definite programming* problem, which can be solved efficiently using, e.g., well-known software toolboxes such as SeDuMi [20]. Based on the solution of the relaxed optimization problem, a suitable algorithm will be devised in Section IV, which is able to obtain near-optimal PEF coefficients that offer *almost* the same performance as the optimal PEF coefficients resulting from the original problem formulation (45), as will be shown in Section V.

Finally, we note that we could easily extend the above considerations to the case where there is only a single PEF $\mathbf{f} \triangleq [f[0], \ldots, f[L_f-1]]^H$ of length $L_f$ that is shared by all transmit antennas (e.g., for reasons of complexity). To this end, we would have to replace the matrices $\mathbf{B}_\bullet$, $\mathbf{D}(\omega)$, and $\boldsymbol{\Upsilon}$ in (45) by effective matrices $\mathbf{B}_{\bullet,eff} \triangleq \sum_{m=1}^{M} \mathbf{B}_{m,\bullet}$, $\mathbf{D}_{eff}(\omega) \triangleq \sum_{m=1}^{M} \lambda_m(\omega)\mathbf{d}(\omega)\mathbf{d}^H(\omega)$, and $\boldsymbol{\Upsilon}_{eff} \triangleq \sum_{m=1}^{M} \boldsymbol{\Upsilon}_m$, respectively [8], where '$\bullet$' stands for '0', '$pre$' or '$post$'. For reasons of conciseness, we focus here on the problem formulation (45) with a separate PEF for each transmit antenna. In Section V, we will address the issue of complexity reduction from a different viewpoint.

## IV. Solution of Optimization Problem

In this section, we provide an algorithm to find a close-to-optimal solution for optimization problem (45). We first rewrite (45) in terms of an equivalent real-valued representation (since not all optimization solvers support complex-valued variables) and then solve it by using semi-definite relaxation and semi-definite programming techniques.

*Real-valued representation:* Recall that vector $\mathbf{f}$ in optimization problem (45) is complex-valued. Let $\mathbf{x}$ and $\mathbf{y}$ denote the real and imaginary parts of vector $\mathbf{f}$. We thus have

$$\mathbf{f} = \mathbf{x} + j\,\mathbf{y}. \tag{46}$$

For notational simplicity, we define

$$\mathbf{z} \triangleq \begin{bmatrix} \mathbf{x} \\ \mathbf{y} \end{bmatrix}. \tag{47}$$

By using simple calculus, we can obtain *real-valued* matrices $\boldsymbol{\Phi}_0$, $\boldsymbol{\Phi}_{pre}$, and $\boldsymbol{\Phi}_{post}$ of size $2ML_f \times 2ML_f$ from $\mathbf{B}_0$, $\mathbf{B}_{pre}$, and $\mathbf{B}_{post}$, respectively, such that

$$\mathbf{f}^H \mathbf{B}_0^H \mathbf{B}_0 \mathbf{f} = \mathbf{z}^T \boldsymbol{\Phi}_0 \mathbf{z}, \tag{48}$$

$$\mathbf{f}^H \mathbf{B}_{pre}^H \mathbf{B}_{pre}\, \mathbf{f} = \mathbf{z}^T \boldsymbol{\Phi}_{pre} \mathbf{z}, \tag{49}$$

$$\mathbf{f}^H \mathbf{B}_{post}^H \mathbf{B}_{post}\, \mathbf{f} = \mathbf{z}^T \boldsymbol{\Phi}_{post} \mathbf{z}. \tag{50}$$

We can also obtain real-valued matrices $\boldsymbol{\Gamma}(\omega_\mu)$ from $\mathbf{D}(\omega_\mu)$ ($\mu = 1, ..., K$) and a real-valued matrix $\boldsymbol{\Lambda}$ from $\boldsymbol{\Upsilon}$ (all of size $2ML_f \times 2ML_f$) such that

$$\mathbf{f}^H \mathbf{D}(\omega_\mu) \mathbf{f} = \mathbf{z}^T \boldsymbol{\Gamma}(\omega_\mu) \mathbf{z}, \qquad \mu = 1, \ldots, K, \tag{51}$$

and

$$\mathbf{f}^H\ \boldsymbol{\Upsilon}\ \mathbf{f} = \mathbf{z}^T \boldsymbol{\Lambda} \mathbf{z}. \tag{52}$$

We are now ready to rewrite problem (45) as the following problem over *real-valued* variables:

$$\begin{aligned} \max_{\mathbf{z}} \quad & \mathbf{z}^T \boldsymbol{\Phi}_0 \mathbf{z} \\ \text{s.t.} \quad & \mathbf{z}^T \left(\boldsymbol{\Phi}_{pre} + \boldsymbol{\Phi}_{post}\right) \mathbf{z} \le \alpha, \\ & \mathbf{z}^T\, \boldsymbol{\Gamma}(\omega_\mu)\, \mathbf{z} \le m(\Omega_\mu), \qquad \mu = 1, \ldots, K, \\ & \mathbf{z}^T\, \boldsymbol{\Lambda}\, \mathbf{z} \le P^{\max}. \end{aligned} \tag{53}$$

We note that problems (45) and (53) are *equivalent*. In fact, their solutions can be converted into each other through the relationship in (46). Problem (53) is a real-valued non-concave quadratic maximization problem. Next, we will explain how we can solve (53) with an acceptable accuracy.

*Semi-definite Relaxation:* We introduce a new real-valued matrix $\mathbf{W}$ such that

$$\mathbf{W} \triangleq \mathbf{z}\,\mathbf{z}^T. \tag{54}$$

Clearly, matrix $\mathbf{W}$ is positive semi-definite (i.e., $\mathbf{W} \succeq \mathbf{0}$) and has unit rank. We also note that for any $(2ML_f \times 2ML_f)$-Hermitian matrix $\mathbf{A}$, we have

$$\mathbf{z}^T\ \mathbf{A}\ \mathbf{z} = \mathrm{trace}\left(\mathbf{A}\ \mathbf{W}\right). \tag{55}$$

Therefore, problem (53) is equivalent to

$$\begin{aligned} \max_{\mathbf{W} \succeq \mathbf{0}} \quad & \mathrm{trace}\left(\boldsymbol{\Phi}_0\ \mathbf{W}\right) \\ \text{s.t.} \quad & \mathrm{trace}\left(\left(\boldsymbol{\Phi}_{pre} + \boldsymbol{\Phi}_{post}\right) \mathbf{W}\right) \le \alpha, \\ & \mathrm{trace}\left(\boldsymbol{\Gamma}(\omega_\mu)\ \mathbf{W}\right) \le m(\Omega_\mu), \quad \mu = 1, \ldots, K, \\ & \mathrm{trace}(\boldsymbol{\Lambda}\ \mathbf{W}) \le P^{\max}, \\ & \mathrm{rank}(\mathbf{W}) = 1. \end{aligned} \tag{56}$$

Problem (56) is still as difficult as problem (53), due to the rank constraint $\mathrm{rank}(\mathbf{W}) = 1$.[5] Therefore, we *discard* the rank constraint in the next step and consider the following *relaxed* optimization problem:

$$\begin{aligned} \max_{\mathbf{W} \succeq \mathbf{0}} \quad & \mathrm{trace}\left(\boldsymbol{\Phi}_0\ \mathbf{W}\right) \\ \text{s.t.} \quad & \mathrm{trace}\left(\left(\boldsymbol{\Phi}_{pre} + \boldsymbol{\Phi}_{post}\right) \mathbf{W}\right) \le \alpha, \\ & \mathrm{trace}\left(\boldsymbol{\Gamma}(\omega_\mu)\ \mathbf{W}\right) \le m(\Omega_\mu), \quad \mu = 1, \ldots, K, \\ & \mathrm{trace}(\boldsymbol{\Lambda}\ \mathbf{W}) \le P^{\max}. \end{aligned} \tag{57}$$

Problem (57) is a *semi-definite programming* (SDP) problem [22]. SDP is a generalization of *linear programming* (LP) over matrices (rather than vectors as in LP). Several solvers, such as SeDuMi [20] can efficiently solve the SDP problem in (57). Next, we will explain how solving problem (57) can help us to find close-to-optimal solutions for problem (56).

*PEF Design Algorithm:* Let $\mathbf{W}^\star$ denote the optimal solution for SDP problem (57). Clearly, if $\mathrm{rank}(\mathbf{W}) = 1$, then the optimal solution $\mathbf{z}^\star$ for problem (56) can be obtained by using *eigenvalue decomposition* of matrix $\mathbf{W}^\star$. If $\mathrm{rank}(\mathbf{W}) > 1$, then we can still obtain a close approximation of $\mathbf{z}^\star$ (and also for $\mathbf{x}^\star$ and $\mathbf{y}^\star$) by using the following steps which are based on the recent results in [23], [24]:

- **Step 1.** Using eigenvalue decomposition, obtain matrix $\mathbf{U}$ such that $\mathbf{W}^\star = \mathbf{U}^\star\, \mathbf{U}^{\star T}$:

  $$\mathbf{W}^\star = \mathbf{V}^{\star T}\, \boldsymbol{\Sigma}^\star\, \mathbf{V}^\star \quad \Rightarrow \quad \mathbf{U}^\star = \mathbf{V}^{\star T}\, \boldsymbol{\Sigma}^{\star \frac{1}{2}},$$

  where $\mathbf{V}^\star$ is a *unitary* matrix and matrix $\boldsymbol{\Sigma}^\star$ is *diagonal*.

[5] The same problem structure has, e.g., also been encountered in the context of beamforming for multiple-antenna relays, see Problem (20) in [21].

- **Step 2.** Using eigenvalue decomposition, obtain unitary matrix $\boldsymbol{\Theta}^\star$ such that $\boldsymbol{\Theta}^{\star T}\ \mathbf{U}^{\star T}\ \boldsymbol{\Phi}_0\ \mathbf{U}^\star\ \boldsymbol{\Theta}^\star$ becomes *diagonal*:

$$\mathbf{U}^{\star T}\boldsymbol{\Phi}_0\mathbf{U}^\star=\boldsymbol{\Theta}^\star\boldsymbol{\Xi}^\star\boldsymbol{\Theta}^{\star T}\ \Rightarrow\ \boldsymbol{\Xi}^\star=\boldsymbol{\Theta}^{\star T}\mathbf{U}^{\star T}\boldsymbol{\Phi}_0\mathbf{U}^\star\boldsymbol{\Theta}^\star,$$

where $\boldsymbol{\Xi}^\star$ is a *diagonal* matrix.

- **Step 3.** Let $\zeta_i$, $i=1,\ldots,2ML_f$, be i.i.d. random variables taking values $-1$ and $+1$ with equal probabilities. Also, let $\boldsymbol{\zeta}=(\zeta_1,\ldots,\zeta_{2ML_f})$. We select

$$\mathbf{z}^\star=\begin{bmatrix}\mathbf{x}^\star\\ \mathbf{y}^\star\end{bmatrix}=\frac{1}{\kappa_{\max}}\mathbf{U}^\star\ \boldsymbol{\Theta}^\star\ \boldsymbol{\zeta},\tag{58}$$

where

$$\kappa_{\max}=\max\left\{\max_{1\le\mu\le K}\frac{\boldsymbol{\zeta}^T\ \boldsymbol{\Theta}^{\star T}\ \mathbf{U}^{\star T}\ \boldsymbol{\Gamma}(\omega_\mu)\ \mathbf{U}^\star\ \boldsymbol{\Theta}^\star\ \boldsymbol{\zeta}}{m(\Omega_\mu)},\ \frac{\boldsymbol{\zeta}^T\ \boldsymbol{\Theta}^{\star T}\ \mathbf{U}^{\star T}\ \boldsymbol{\Lambda}\mathbf{U}^\star\ \boldsymbol{\Theta}^\star\ \boldsymbol{\zeta}}{P^{\max}},\ \frac{\boldsymbol{\zeta}^T\ \boldsymbol{\Theta}^{\star T}\ \mathbf{U}^{\star T}\ (\boldsymbol{\Phi}_{pre}+\boldsymbol{\Phi}_{post})\mathbf{U}^\star\ \boldsymbol{\Theta}^\star\ \boldsymbol{\zeta}}{\alpha}\right\}.\tag{59}$$

We can verify that for any random choice of vector $\boldsymbol{\zeta}$, the obtained $\mathbf{x}^\star$ and $\mathbf{y}^\star$ in (58) satisfy all the inequality constraints in problem (53). We then simply set

$$\mathbf{f}^\star:=\mathbf{x}^\star+j\,\mathbf{y}^\star.\tag{60}$$

*Optimality Bound:* Let $\mathbf{f}_{opt}$ denote the optimal solution of the PEF design problem in (45). We have

$$\mathbf{f}^{\star H}\mathbf{B}_0^H\mathbf{B}_0\mathbf{f}^\star\le\mathbf{f}_{opt}^H\mathbf{B}_0^H\mathbf{B}_0\mathbf{f}_{opt}\le\operatorname{trace}\left(\boldsymbol{\Phi}_0\mathbf{W}^\star\right),\tag{61}$$

where the last inequality is valid because problem (57) is *less restrictive* than problem (45). From (61), the *optimality loss* when using $\mathbf{f}^\star$ instead of $\mathbf{f}_{opt}$ is upper-bounded as

$$\begin{aligned}\frac{\mathbf{f}_{opt}^H\mathbf{B}_0^H\mathbf{B}_0\mathbf{f}_{opt}-\mathbf{f}^{\star H}\mathbf{B}_0^H\mathbf{B}_0\mathbf{f}^\star}{\mathbf{f}_{opt}^H\mathbf{B}_0^H\mathbf{B}_0\mathbf{f}_{opt}}&=1-\frac{\mathbf{f}^{\star H}\mathbf{B}_0^H\mathbf{B}_0\mathbf{f}^\star}{\mathbf{f}_{opt}^H\mathbf{B}_0^H\mathbf{B}_0\mathbf{f}_{opt}}\\&\le 1-\frac{\mathbf{f}^{\star H}\mathbf{B}_0^H\mathbf{B}_0\mathbf{f}^\star}{\operatorname{trace}\left(\boldsymbol{\Phi}_0\mathbf{W}^\star\right)}.\end{aligned}\tag{62}$$

By using the upper bound in (62), we have verified through simulations that the optimality loss for the proposed design algorithm is usually very small (see Section V). Thus, a PEF design based on the coefficients $\mathbf{f}^\star$ has *almost* the same performance as that achieved with the optimal coefficients $\mathbf{f}_{opt}$. Moreover, by following the analysis in [25], we can show that the optimality loss is *always* guaranteed to be less than 36%.

## V. Numerical Results

In this section, we assess the performance of our proposed PEF scheme via simulations and compare it with pure pre-Rake combining (i.e., *without* any pre-equalization) [3]–[6], [9] and the symbol-level minimum-mean-squared-error (MMSE) PEF scheme in [8]. For each transmitter structure, we assume that all-pre-Rake combining according to (5) is applied. Moreover, no equalizer is employed at the receiver, as explained in Section II.

Unless stated otherwise, our simulation setting is as follows. The operational bandwidth is $B_s=1$ GHz with $\Omega_{\min}=2\pi\times3.5$ GHz and $\Omega_{\max}=2\pi\times4.5$ GHz [10], i.e., $K=1001$. The spectral mask $m(\Omega)$ is assumed to be flat within this area (cf. Fig. 2). We set the filter length for the optimal PEFs to $L_f=5$, the spreading factor to $N=6$, $\eta_{pre}=\eta_{post}=\lfloor\frac{L_t}{2}\rfloor$, and $\alpha=\sigma_s^2$. Throughout, we focus on transmitter structures with one or two transmit antennas ($M=1,2$). For a fair comparison between the cases $M=1$ and $M=2$, we set the maximum transmit power level to $P^{\max}=1$ in all cases (irrespective of the number of transmit antennas). For brevity, we only include simulation results for channel model CM1, where the parameters are as in [14]. The results for CM2, CM3, and CM4 are similar, however. All simulation results have been obtained based on 100 statistically independent channel realizations. In the case of two transmit antennas ($M=2$), we assume that the lognormal terms $\vartheta_1$ and $\vartheta_2$ are correlated with a correlation coefficient of 0.86 [16].

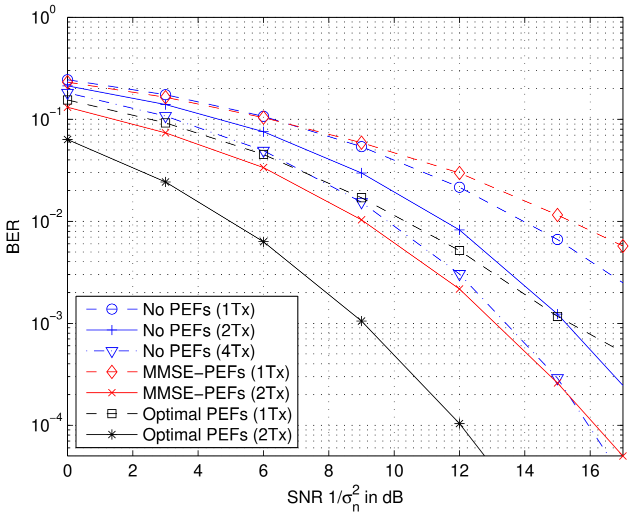


Fig. 3. Bit error rate (BER) vs. $1/\sigma_n^2$ for the proposed optimal PEF scheme ($L_f=5$), the MMSE-PEF scheme [8] ($L_f=10$, with power back-off), and pure pre-Rake combining [2] (with power back-off). The latter two schemes do not take any spectral mask considerations into account. All numerical results are for an operational bandwidth of $B_s=1$ GHz and a spreading factor of $N=6$.

*Performance Comparison:* In Fig. 3, the BER performance of the designed PEF scheme is compared with pure all-pre-Rake combining ('No PEFs') and the symbol-level MMSE-PEF scheme ('MMSE-PEFs'). In order to avoid violating the spectral mask constraints in the case of pure pre-Rake combining and the symbol-level MMSE-PEF scheme, we have applied appropriate power back-offs for each channel realization. Note that no power back-offs are needed for our optimal PEF design, as we take the spectral mask into account in the optimization procedure. First, we note that the proposed optimal PEF scheme (as well as the symbol-level MMSE-PEF scheme) offers significant combining gains when multiple transmit antennas are employed, despite the rather large correlation factor between the lognormal shadowing terms. Moreover, we can see that our designed optimal PEF scheme significantly outperforms pure pre-Rake combining as well as the symbol-level MMSE-PEF scheme (even though twice the filter length has been employed for the latter). Interestingly, the performance of the MMSE-PEF scheme for $M=1$ ('1Tx') is even slightly worse than the performance with pure pre-Rake combining, which is due to less favorable power-back-off factors in this example. For $M=2$ ('2Tx'), however, the MMSE-PEF scheme outperforms pure pre-Rake combining, as it tends to suffer from a smaller amount of residual ISI and thus offers better combining gains. Still, the performance of the MMSE-PEF scheme is relatively poor compared to the

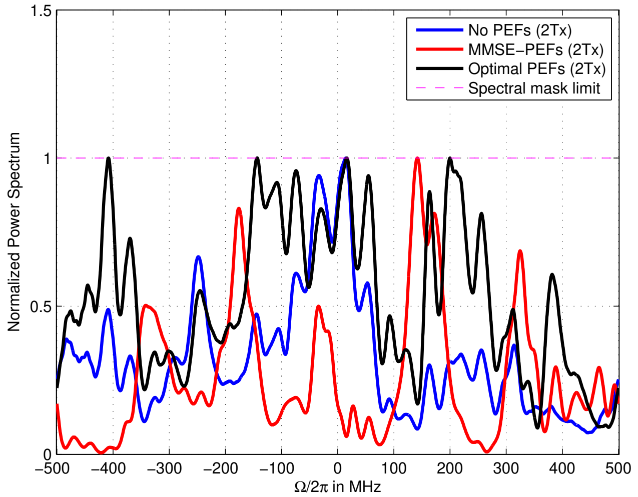


Fig. 4. Transmitted sum power spectrum of the transmitted UWB signals in baseband representation within the $B_s = 1$ GHz bandwidth for the proposed optimal PEF scheme ($L_f = 5$), the symbol-level MMSE-PEF design [8] ($L_f = 10$, with power back-off), and pure pre-Rake combining [2] (with power back-off). The spreading factor was chosen as $N = 6$. Note that only the optimal PEFs obey the spectral mask without requiring any power back-off.

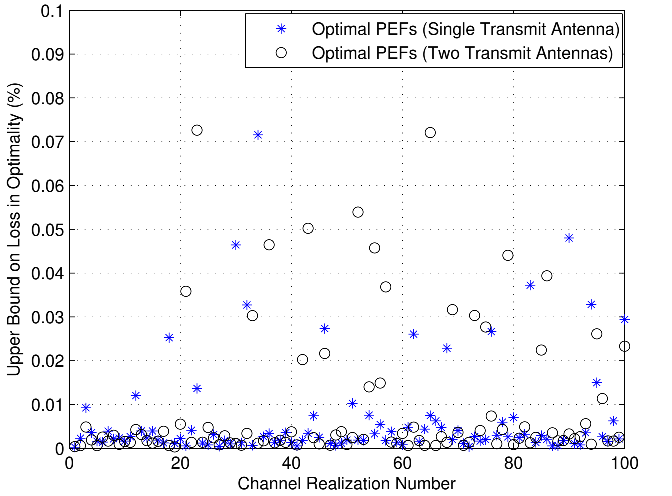


Fig. 5. Upper bound on the loss of optimality in our proposed PEF design with respect to solving optimization problem (45). Here, the results for 100 random channel realizations are shown ($B_s = 1$ GHz, $L_f = 5$, $N = 6$). The upper bound is obtained based on inequality (62). We can see that in the considered examples the PEF designs are always very close to the optimum.

designed optimal PEFs (for $M = 2$, the optimal PEFs offer a gain of about 4.1 dB at a BER of $10^{-4}$), which is again due to the power-back-off factors applied in the case of the MMSE-PEF scheme. Concerning pure pre-Rake combining, we can see that increasing the number of transmit antennas does not help as much as in the case of the optimal PEF scheme or the MMSE-PEF scheme. For example, if $M = 4$ transmit antennas are employed, the performance of pure pre-Rake combining is still 3.8 dB away from the performance of the designed optimal PEFs with $M = 2$ transmit antennas (at a BER of $10^{-4}$).

*Obeying Spectral Mask:* For the case of $M = 2$ transmit antennas and a random channel realization, the sum power spectra of the transmitted baseband UWB signals for the three transmitter structures are shown in Fig. 4, where we again applied suitable power-back-off factors in the case of pure pre-Rake combining and the symbol-level MMSE-PEF scheme. For simplicity, we have normalized the spectral mask level to one. We can see that our designed PEFs lead to a transmitted sum power spectrum that fully obeys the spectral mask. Moreover, at multiple frequencies, the resulting sum power spectrum is close to the spectral mask limit or even touches it. In comparison, the transmitted sum power spectra for pure pre-Rake combining and the symbol-level MMSE-PEF design look more ‘peaky’. In conjunction with the mandatory power-back-off factor, this leads to comparatively low overall transmit powers, as can be seen from the areas under the corresponding transmitted sum power spectra. This explains the inferior performance of pure pre-Rake combining and the symbol-level MMSE-PEF design compared to the optimal PEFs.

*Near-Optimality:* Recall that the semi-definite relaxation discussed in Section IV may lead to some loss in optimality in our PEF design with respect to solving the original problem (45). In general, it is difficult to obtain the exact loss of optimality in each simulated scenario. However, inequality (62) can help to obtain an *upper bound* on the loss of optimality. Corresponding results are shown in Fig. 5 for 100 random channel realizations (both for $M = 1$ and $M = 2$ transmit antennas). We can see that our PEF design is very close to the optimum for all considered cases (less than 0.08% loss). Hence, the PEF design based on the relaxed optimization problem has *almost* the same performance as a PEF design based on the original optimization problem (45).

*Impact of the Spreading Factor:* Fig. 6 shows the BER performance of the designed optimal PEF scheme as a function of the spreading factor $N$ (both for $M = 1$ and $M = 2$ transmit antennas). It can be seen that the BER performance improves only slightly when the spreading factor $N$ is increased beyond $N = 6$. Thus with regard to the effective data rate, which drops linearly with the spreading factor, $N = 6$ appears to be a reasonable choice. On the other hand, the effective data rate can be further increased by lowering the spreading factor, which comes at the expense of a rather small performance degradation, as long as we choose, say, $N \geq 4$.

*Complexity Reduction:* Although we tackled the non-convexity in optimization problem (45) by using a semi-definite relaxation technique in Section IV, solving the resulting semi-definite program can still be time consuming, due to the large number of spectral mask constraints (e.g., $K = 1001$ given a system bandwidth of $B_s = 1$ GHz). Fig. 7 shows the BER performance of the optimum PEF design as a function of the number of spectral mask constraints (in %) included in the optimization procedure. The spectral mask constraints are always placed at frequencies which *uniformly* spread out over the operational bandwidth $B_s$. For example, if only 10% of the constraints are included in the PEF design optimization problem (45), these constraints are placed at frequencies $\mu_1, \mu_{11}, \ldots, \mu_{991}, \mu_{1001}$. Clearly, in this case the sum power spectrum of the transmitted signals *may* violate the spectral mask limit at *other* frequencies, e.g., at $\mu_2, \ldots \mu_{10}$. This requires applying an appropriate *power back-off*, where needed (similarly to the case of pure pre-Rake combining and the symbol-level MMSE-PEF design). As a result, the BER performance degrades when fewer constraints are included. Interestingly though, this performance degradation is rather graceful, as long as the number of spectral mask constraints is not too small. For example, when including only 10% of all spectral mask constraints, the resulting performance loss is still negligible (both for $M = 1$ and $M = 2$ transmit antennas).

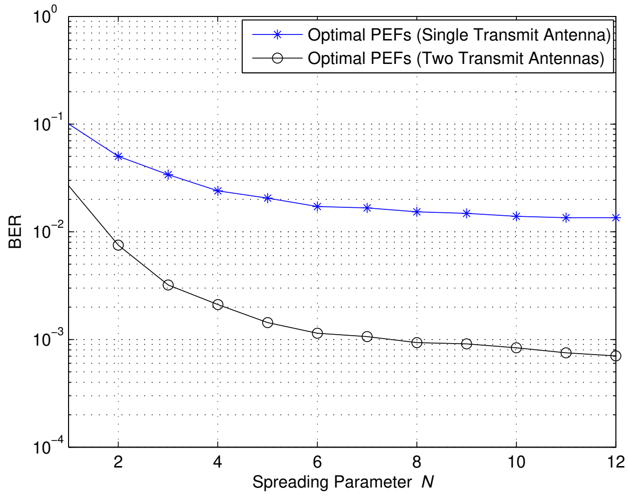


Fig. 6. BER performance of the optimum PEF design as a function of the spreading factor $N$ ($B_s = 1$ GHz, $L_f = 5$, $1/\sigma_n^2 = 9$ dB).

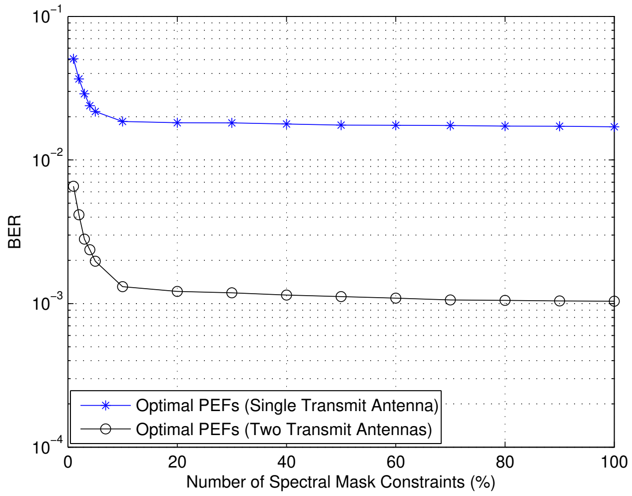


Fig. 7. BER performance of the optimum PEF design as a function of the number of spectral mask constraints (in %) included in the optimization procedure ($B_s = 1$ GHz, $L_f = 5$, $N = 6$, $1/\sigma_n^2 = 9$ dB).

This is due to the fact that the resulting sum power spectra are usually *smooth*. On the other hand, a reduction from 100% to 10% of spectral mask constraints will lead to a significant reduction in computation time, which renders the proposed PEF design more suitable for an implementation in practice.

## VI. Conclusions

We proposed a novel optimization-based PEF design framework for MISO DS-UWB systems with pre-Rake combining. Unlike the previous work on pre-equalizer and pre-Rake filter design in the existing literature, we explicitly took into account the spectral mask constraints, which are usually imposed by the telecommunications standardization and regulation bodies around the world. As a result, our design avoids the need for an inefficient power back-off, which is necessary for existing pre-filter designs in order to conform the spectral mask constraints. Simulation results confirmed that the proposed PEF design leads to significant performance gains over PEF structures without explicit spectral mask considerations. In particular, it was shown to offer a close-to-optimal performance. The use of multiple transmit antennas was shown to offer significant combining gains, even in the presence of fairly large shadowing correlations. The complexity of the scheme can be reduced significantly by selecting only a (suitable) subset of all spectral mask constraints within the operational bandwidth, which usually comes at the expense of a rather small performance degradation. Finally, we note that the PEF design has the capability of adhering to spectral masks with arbitrary shapes, although we have focused on a flat spectral mask throughout this paper.

## References


[1] M. Win and R. Scholtz, "Characterization of Ultra-Wide Bandwidth Wireless Indoor Channels: A Communication-Theoretic View," *IEEE J. Select. Areas Commun.*, vol. 20, pp. 1613–1627, Dec. 2002.

[2] T. Strohmer, M. Emami, J. Hansen, G. Papanicolaou, and A. Paulraj, "Application of Time-Reversal with MMSE Equalizer to UWB Communications," in *Proc. of IEEE Globecom*, Dallas, TX, Nov. 2004.

[3] H. Nguyen, I. Kovacs, and P. Eggers, "A Time Reversal Transmission Approach for Multiuser UWB Communications," *IEEE Trans. Antennas and Propagation*, vol. 54, pp. 3216–3224, Nov. 2006.

[4] Y.-H. Chang, S.-H. Tsai, X. Yu, and C.-C. Kuo, "Ultrawideband Transceiver Design Using Channel Phase Precoding," *IEEE Trans. Signal Processing*, vol. 55, pp. 3807–3822, July 2007.

[5] R. Qiu, C. Zhou, N. Guo, and J. Zhang, "Time Reversal with MISO for Ultrawideband Communications: Experimental Results," *IEEE Antennas and Wireless Propagation Letters*, vol. 5, pp. 269–273, Dec. 2006.

[6] W. Cao, A. Nallanathan, and C. Chai, "On the Tradeoff between Data Rate and BER Performance of Pre-RAKE DS UWB System," in *Proc. of IEEE Globecom*, San Francisco, CA, Nov. 2006.

[7] M. Emami, M. Vu, J. Hansen, A. Paulraj, and G. Papanicolaou, "Matched Filtering with Rate Back–Off for Low Complexity Communications in Very Large Delay Spread Channels," in *Proc. of the 38th Asilomar Conf. Signals, Systems, and Computers*, Pacific Grove, CA, Nov. 2004.

[8] E. Torabi, J. Mietzner, and R. Schober, "Pre-Equalization for MISO DS-UWB Systems with Pre-Rake Combining," *IEEE Trans. Wireless Commun.*, vol. 8, pp. 1295–1307, Mar. 2009.

[9] K. Usuda, H. Zhang, and M. Nakagawa, "Pre-Rake Performance for Pulse Based UWB System in a Standardized UWB Short-Range Channel," in *Proc. of IEEE WCNC*, Atlanta, GA, Mar. 2004.

[10] R. Fisher, R. Kohno, M. McLaughlin, and M. Welbourn, "DS–UWB Physical Layer Submission to IEEE 802.15 Task Group 3a (Doc. Number P802.15-03/0137r4)," Jan. 2005.

[11] IEEE P802.15–TG4a, "Part 15.4: Wireless Medium Access Control (MAC) and Physical Layer (PHY) Specifications for Low-Rate Wireless Personal Area Networks (LR-WPANs): Amendment to Add Alternate PHY," Jan. 2007.

[12] A.-H. Mohsenian-Rad, J. Mietzner, R. Schober, and V. Wong, "Pre-Equalization for DS-UWB Systems with Spectral Mask Constraints," in *Proc. of IEEE ICC*, Cape Town, South Africa, May 2010.

[13] X. Wu, Z. Tian, T. N. Davidson, and G. B. Giannakis, "Optimal Waveform Design for UWB Radios," *IEEE Trans. Signal Processing*, vol. 54, no. 6, pp. 2009–2021, June 2006.

[14] Channel Modeling Sub-Committee Final Report, "IEEE 802.15-02/368r5-SG3a, IEEE P802.15," Dec. 2002.

[15] A. Molisch, J. Foerster, and M. Pendergrass, "Channel Models for Ultrawideband Personal Area Networks," *IEEE Wireless Communications*, vol. 10, pp. 14–21, Dec. 2003.

[16] Z. Lin, X. Peng, K. Png, and F. Chin, "Kronecker Modelling for Correlated Shadowing in UWB MIMO Channels," in *Proc. of the IEEE WCNC*, Hong Kong, Mar. 2007.

[17] "FCC Notice of Proposed Rule Making, Revision of Part 15 of the Commission's Rules Regarding Ultrawideband Transmission Systems," Communications Commission ET-Docket 98-153, May 2003.

[18] A. Oppenheim and R. Schafer, *Digital Signal Processing*. Englewood Cliffs, New Jersey: Prentice–Hall, Inc., 1975.

[19] S. Boyd and L. Vandenberghe, *Convex Optimization*. Cambridge University Press, 2004.

[20] I. Polik, "SeDuMi User Guide," http://sedumi.ie.lehigh.edu, June 2005.

[21] R. Zhang, Y.-C. Liang, C. C. Chai, and S. Cui, "Optimal Beamforming for Two-Way Multi-Antenna Relay Channel with Analogue Network Coding," *IEEE J. Select. Areas Commun.*, to appear, 2010.

[22] L. Vandenberghe and S. Boyd, "Semidefinite Programming," *SIAM Review*, vol. 38, pp. 49–95, Mar. 1996.

[23] S. He, Z. Q. Luo, J. Nie, and S. Zhang, "Semidefinite Relaxation Bounds for Indefinite Homogeneous Quadratic Optimization," *SIAM Journal on Optimization*, vol. 19, pp. 503–523, June 2008.

[24] A. Nemirovski, C. Roos, and T. Terlaky, "On Optimization of Quadratic Form over Intersection of Ellipsoids with Common Center," *Mathematical Programming*, vol. 86, pp. 463–473, June 1999.

[25] Y. Nesterov, "Semidefinite Relaxation and Non-Convex Quadratic Optimization," *Optimization Methods and Software*, vol. 12, pp. 1–20, 1997.